SUPPORTING INFORMATION FOR:

Multivalent Ligand Binding to Cell Membrane Antigens: Defining the Interplay of Affinity, Valency, and Expression Density

Clifford M. Csizmar[1], Jacob R. Petersburg[1], Thomas J. Perry[1], Lakmal Rozumalski[1], Benjamin J. Hackel[2] & Carston R. Wagner[1]*

[1]Department of Medicinal Chemistry
[2]Department of Chemical Engineering and Materials Science
University of Minnesota, Minneapolis, MN 55455

*Corresponding author
Carston R. Wagner
2231 6th St. SE
Minneapolis, MN 55455
wagne003@umn.edu

TABLE OF CONTENTS

Table S1. CSAN Apparent Affinities, Cooperativity, and Enhancement Parameters 2

Table S2. Predicted versus Experimental CSAN Apparent Affinities 3

Figure S1. SEC Demonstrating CSAN Oligomerization with bisMTX 4

Figure S2. DLS Characterization of Key CSAN Species 5

Figure S3. Selectivity of Fibronectin Functionalized CSANs 6

Figure S4. Un-Normalized Binding Isotherms for Fibronectin Functionalized CSANs 7

Figure S5. Model of Antigen Accessibility 8

Figure S6. Target Discrimination Across a Range of Ligand Concentrations 11

Figure S7. SEC Demonstrating CSAN Oligomerization with DOTA-bisMTX 12

Figure S8. CSAN Biodistribution in a Murine Dual-Xenograft Model 13

Appendix S1. Fusion Protein Sequences 14

References 16

Clone	Valency (N)	$K_{d,N}$ (nM)	α	$1/\beta$
C5	1	500 ± 60	1.0	1.0
	2	140 ± 40	2.9×10^{-1}	3.7
	4	33 ± 8	2.9×10^{-2}	15
	8	6.9 ± 1.8	3.0×10^{-4}	72
B22	1	1,600 ± 200	1.0	1.0
	2	400 ± 100	2.6×10^{-1}	3.9
	4	150 ± 80	2.1×10^{-2}	10
	8	20 ± 11	1.2×10^{-4}	78

Table S1. Apparent Affinity, Cooperativity, and Enhancement Parameters of Multivalent CSANs. Apparent $K_{d,N}$ values (nM) for the data presented in **Figure 3** of the main text are provided. Each titration was performed at least three times, and data is presented as the mean ± standard deviation of the $K_{d,N}$ values resulting from these independent trials. The cooperativity (α) of the CSANs was calculated using ***equation 2*** of the main text; the values <1 indicate the CSANs are negatively-cooperative. Enhancement factors (β) were calculated using ***equation 3*** of the main text; values are presented as $1/\beta$ to enable direct interpretation as the fold improvement in the multivalent apparent $K_{d,N}$ value over that of the singly-targeted $K_{d,1}$ value.

#	Valency	Fn3 Clone	Target Cell	Predicted $K_{d,N}$ (nM)	Experimental $K_{d,N}$ (nM)
1	4	C5	MDA-MB-231	125	150
2	4	C5	LNCaP	32	34
3	4	B22	LNCaP	103	74
4	8	B22	LNCaP	26	21

Table S2. Comparison of Predicted and Experimental Dissociation Constants. The accuracy of ***equation 2*** was tested by comparing predicted $K_{d,N}$ values to experimentally determined values. Notably, these experimental values were not used to create ***equation 2*** and thus comprise a unique set of conditions suitable for testing the equation's predictive capacity. Affinity titrations were performed once and are presented as estimated values without error.

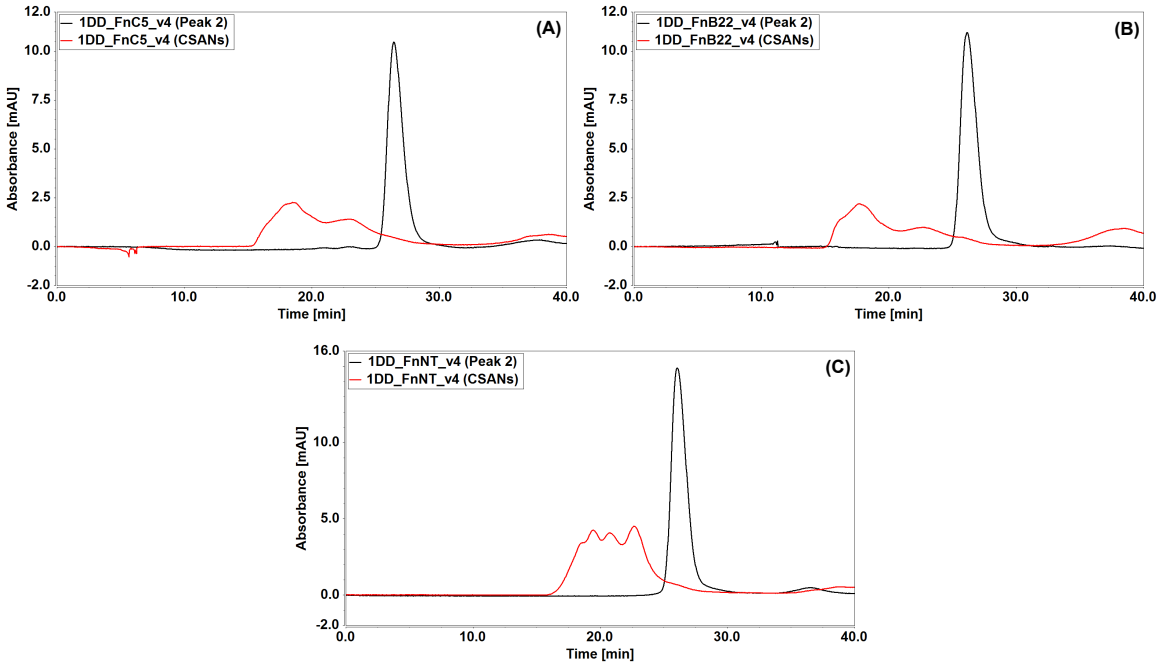

Figure S1. SEC Demonstrates Complete Oligomerization of DHFR^2-Fn3 Monomers into CSANs. Purified DHFR^2-Fn3 monomers (black) were analyzed by SEC, as described in the main text. For oligomerization, a 3-fold molar excess of bisMTX was added to a solution of monomeric protein and, after ≥30 min incubation at room temperature, analyzed via SEC in identical fashion. As shown, all three constructs (A) DHFR^2-Fn3 C5, (B) DHFR^2-Fn3 B22, and (C) DHFR^2-Fn3 NT all completely oligomerized into CSANs (red) with no residual monomeric species detected. Previous cryo-EM analyses of these oligomerized species provided direct evidence of nanoring formation.[1, 2]

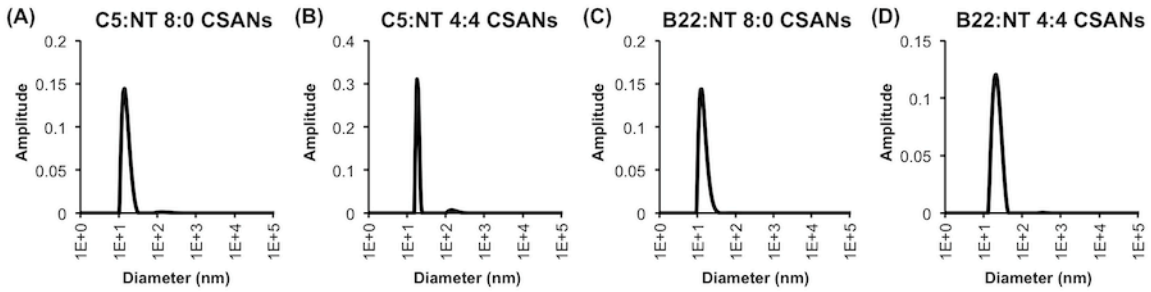

Entry	Targeting Ligand	T:NT Ratio	Hydrodynamic Diameter (nm)	Dispersity
(A)	C5	8:0	17 ± 6.8	40%
(B)	C5	4:4	19 ± 4.9	26%
(C)	B22	8:0	18 ± 6.6	38%
(D)	B22	4:4	19 ± 14	72%

Figure S2. DLS Characterization of Key CSAN Species. For analysis, 60 µL of CSANs in PBS was loaded into a cuvette and analyzed on a Punk DLS unit (Unchained Labs). Hydrodynamic diameter values represent the mean ± standard deviation of at least three measurements. These results compare favorably with our previously-reported DLS analysis of other Fn3-targeted CSANs.[1]

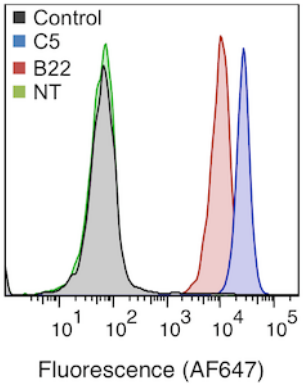

Figure S3. Selectivity of Fibronectin Functionalized CSANs. Separately, the $DHFR^2$-C5, $DHFR^2$-B22, and $DHFR^2$-NT subunits were oligomerized into CSANs and assessed to their binding to EpCAM-positive cells via flow cytometry, as described in the main text. Briefly, $5x10^4$ EpCAM-expressing MCF-7 cells were washed with PBSA and labeled with 100 nM CSANs for 90 min at 4 ºC. Cells were then pelleted (8,000 g, 30 s, 4 ºC) and resuspended in 50 µL anti-His antibody (clone 4E3D10H2/E3) Alexa Fluor 647 conjugate (50 µg/mL in PBSA). After incubating at 4 ºC for ≥30 min in the dark, cells were washed thrice with 1 mL cold PBSA before the fluorescence was analyzed on an LSR II flow cytometer (BD Biosciences). As shown, the EpCAM targeted CSANs utilizing either Fn3 clone C5 (blue) or clone B22 (red) exhibit robust binding to the MCF-7 cells, with fluorescent signals directly proportional to their respective apparent affinities. In contrast, the CSANs displaying the non-targeted Fn3 clone NT (green) produce no appreciable fluorescent signal compared to the secondary-only control (black), indicative of a lack of binding.

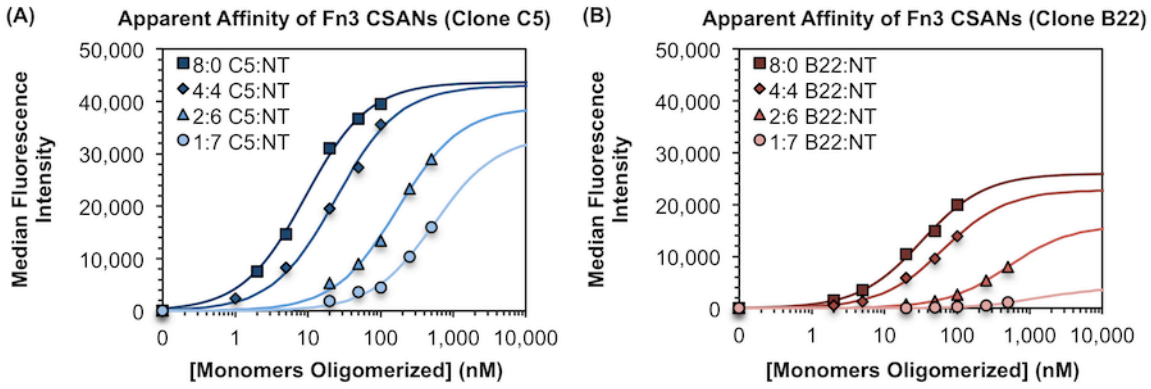

Figure S4. Un-Normalized Binding Isotherms for Fibronectin Functionalized CSANs. Companion data for **Figure 2** of the main text. Here, the median fluorescence intensity (MFI) values are directly plotted against the ligand concentration without any normalization to the theoretical maximum of the binding isotherm. For clarity, data from a single representative titration is shown for each sample. In contrast, the data in **Figure 2** *is* normalized to the fitted maximum value, enabling the determination of the fraction of bound ligand at each concentration and facilitating the direct comparison of replicate titrations.

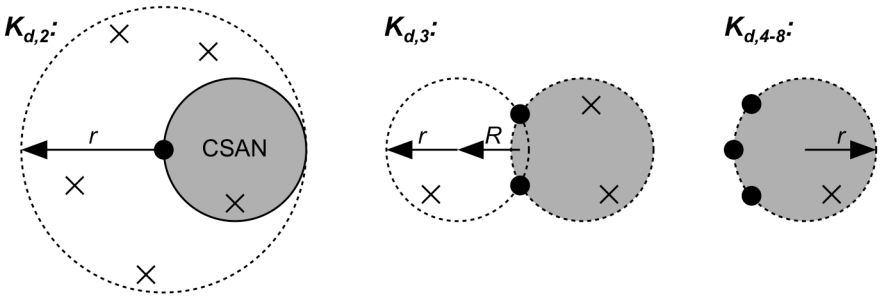

Figure S5. Model of Antigen Accessibility. The number of antigens (i.e., EpCAMs) accessible to the CSAN was modeled for each possible binding event (up to eight for the fully octavalent CSANs). Considering the second binding event ($K_{d,2}$), once the CSAN (grey circle) binds to the first EpCAM (black dot), it can rotate about that binding interaction and access the circular area indicated by the dashed line. The area of this circle can be calculated from the known diameter of the CSAN (~20×10^{-9} m).[1, 2] Assuming an average diameter of 14×10^{-6} m for mammalian cells in suspension[3], the number of EpCAMs (cross marks) present in this area can be calculated using the experimental number of EpCAMs/cell (**Figure 4A-D** in the main text). Provided that the CSAN can access the hemispheric volume above this cell surface area, the effective molarity of EpCAMs in this region can be determined. A similar analysis can be performed for the third binding event ($K_{d,3}$); now that the CSAN is tethered by two ligand/receptor interactions, it is less free to rotate. Making the most generous assumuption about the conformational flexibility of this arrangement, the CSAN can now occupy the area indicated by the partially overlapping circles; likewise, it can access the volume of the corresponding half spindle torus. For the subsequent binding events ($K_{d,4-8}$), the CSAN is very likely anchored in its orientation, and the remaining ligands bind to any accessible EpCAMs in the circular area (smaller hemispheric volume). The calculated EpCAM numbers and effective molarities are presented in **Figure 4F-G** of the main text.

Assumptions and Approximations. This model makes a number of additional assumptions, including: (1) the radius of the cell is much greater than the radius of the CSAN, such that the

surface of the cell is approximated as a planar surface with respect to the CSAN; (2) EpCAM moieties exist as sizeless monomers that are homogenously distributed across the surface of the cell; (3) There is no lateral diffusion of antigens across the cell membrane, as is expected for binding experiments conducted at 4 ºC; (4) the CSAN scaffold itself occupies no space; (5) the linkers that tether the binding domains to the CSAN are sufficiently long and flexible such that the conformational flexibility of the Fn3s is essentially infinite and they can sample the area of the CSAN itself (as opposed to a defined area along the periphery), and (6) each ligand has an equal probability of binding to a cell surface antigen. While these assumptions may or may not be valid, we note that the model derived under these constraints does offer reasonable correlation to the experimental results.

Estimation of Antigen Thresholds. We sought to estimate the minimum EpCAM density required to enable fully octavalent binding of a CSAN to a cell membrane. Using ***equation 1***, the observed $K_{d,N}$ values for fully-targeted (i.e., 8:0 C5:NT) CSANs against the MCF-7 (6.9 ± 1.8 nM), LnCAP (7.2 ± 3.7 nM), SK-OV-3 (19 ± 3.4 nM), and MDA-MB-231 (27 ± 2.8 nM) cells (**Figure 4**) were converted to estimated binding valencies of N = 8, 8, 5, and 4, respectively. This suggested that the CSANs could bind octavalently to the MCF-7 and LNCaP cells, but only pentavalently to the SK-OV-3 cells and tetravalently to the MDA-MB-231 cells. Per **Figure 4F** and the model of EpCAM accessibility discussed above, this pattern of binding is most consistent with a treshold number of accessible antigens between 0.042 – 0.057 EpCAMs, as this “cut off” permits eight binding events for the MCF-7 and LNCaP cells but only five and three for the SK-OV-3 and MDA-MB-231 cells, respectively. Essentially, the threshold may fall anywhere between the fourth and fifth point on the SK-OV-3 curve (green) in **Figure 4F**, which have the respective calculated values of 0.042 and 0.057 EpCAMs. Thus, we estimate the threshold as the midpoint of this range, 0.049 accessible EpCAMs, and represent that value by

the horizontal black dashed line in **Figure 4F**. These numbers of accessible EpCAMs (**Figure 4F**) were calculated using the general equation:

$$(\textbf{Eq. S1})\ R_A = \frac{R}{4\pi r_{cell}^2} \cdot A_L$$

Where R_A is the number of accessible receptors (in this case, EpCAM), R is the number of receptors/cell, r_{cell} is the radius of the cell, and A_L is the area accesible to the ligand (in this case, the CSAN). Note that (1) the A_L term will vary according to the model discussed above, and (2) division of R_A by the volume accessible to the ligand provides the effective concentration of receptors (i.e., $[EpCAM]_{eff}$ in **Figure 4G**).

Using the form of A_L for the eighth binding event ($K_{d,8}$) and rearranging ***equation S1*** enabled conversion of the accessible EpCAM thresholds (R_A = 0.042 – 0.057) to EpCAM/cell values of R = 6.5 – 8.9x10^5 EpCAMs/cell. Via the relationship elucidated in **Figure 4E**, this indicates a 1.6 – 1.8 fold (39 – 45%) reduction in $K_{d,N}$. The midpoint of this threshold region is depicted as the red point in **Figure 4E**, with the upper and lower bounds represented by the projected red dashed lines. A summary of estimated threshold bounds are provided in the table below:

	Accessible EpCAMs	**$[EpCAM]_{eff}$ (μM)**	**EpCAMs/Cell**	**Fold $K_{d,N}$ Reduction**	**% $K_{d,N}$ Reduction**	**Representation in Figure 4E**
Upper Estimate	0.057	45	8.9x10^5	1.6	39%	Dashed red lines
Median Estimate	0.049	39	7.7x10^5	1.7	42%	Solid red point
Lower Estimate	0.042	33	6.5x10^5	1.8	45%	Dashed red lines

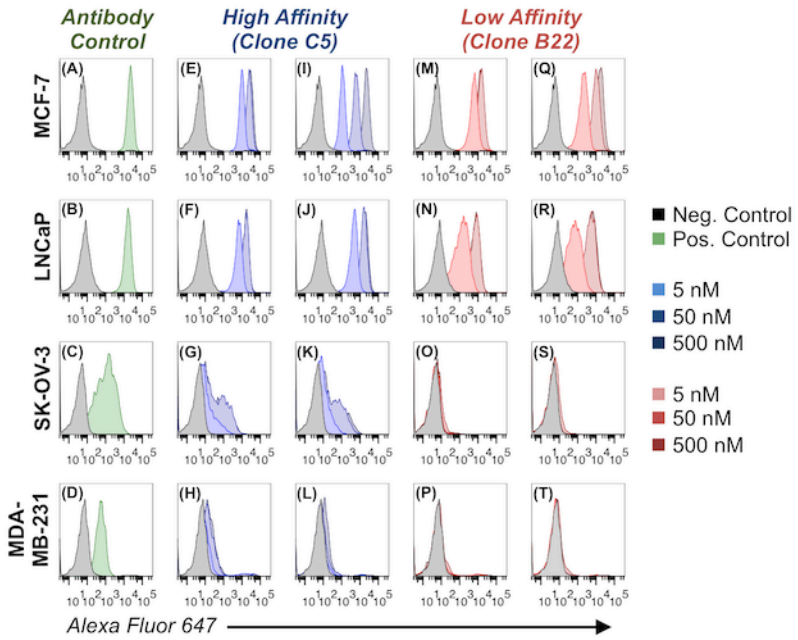

Figure S6. Target Discrimination Across a Range of Ligand Concentrations. Companion data for **Figure 5** of the main text, where the flow cytometry histogram plots depict CSAN binding capability across a 2-log range of concentrations (i.e., 5, 50, and 500 nM).

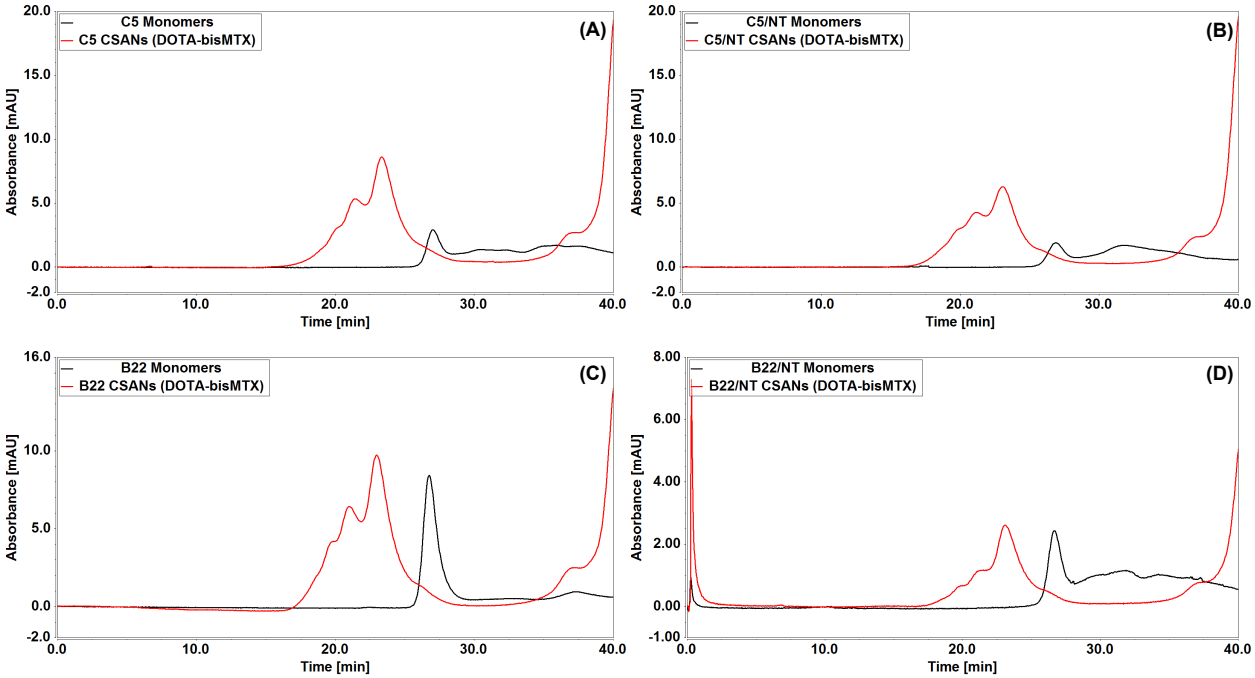

Figure S7. Oligomerization of DHFR^2-Fn3 Monomers into CSANs using DOTA-bisMTX. Purified DHFR^2-Fn3 monomers (black) were analyzed by SEC, as described above. For oligomerization, a 3-fold molar excess of DOTA-bisMTX was added to a solution of monomeric protein and, after ≥30 min incubation at room temperature, analyzed via SEC in identical fashion. As shown, constructs (A) DHFR^2-Fn3 C5, (B) a 1:1 mixture of DHFR^2-Fn3 C5 and DHFR^2-Fn3 NT, (C) DHFR^2-Fn3 B22, and (D) a 1:1 mixture of DHFR^2-Fn3 B22 and DHFR^2-Fn3 NT all completely oligomerized into CSANs (red) with no residual monomeric species detected.

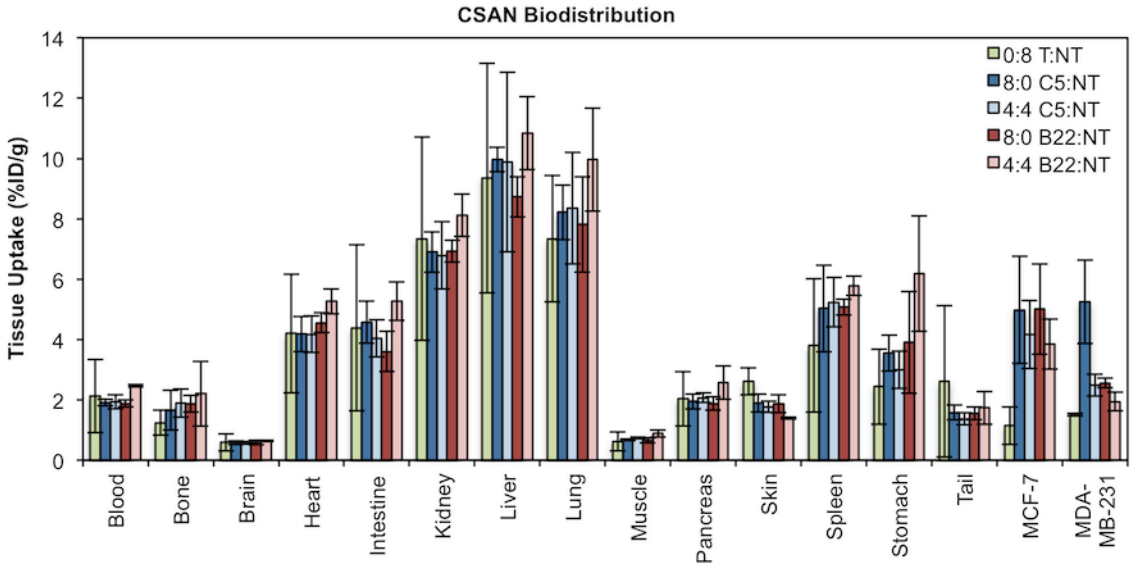

Figure S8. Biodistribution of Avidity-Modulated CSANs. Eighteen hours after the IV infusion of avidity-modulated CSANs, mice were euthanized and tissues were resected, weighed, and measured for activity. Activity values were time-corrected to 18 h to account for continued decay during the weighing/counting process. Data is presented as the mean ± standard deviation of the mice (n = 3) in each treatment group.

APPENDIX S1. FUSION PROTEIN SEQUENCES

DHFR^2-Fn3 (C5) *(497 amino acids; calculated MW 52.9 kDa)*

MGEQKLISEEDLGGSGGGSGGGISLIAALAVDRVIGMENAMPWNLPADLAWFKRNTLNKPVIM
GRHTWESIGRPLPGRKNIILSSQPGTDDRVTWVKSVDEAIAAAGDVPEIMVIGGGRVYEQFLPK
AQKLYLTHIDAEVEGDTHFPDYEPDDWESVFSEFHDADAQNSHSYSFEILERRGGISLIAALAV
DRVIGMENAMPWNLPADLAWFKRNTLNKPVIMGRHTWESIGRPLPGRKNIILSSQPGTDDRVT
WVKSVDEAIAAAGDVPEIMVIGGGRVYEQFLPKAQKLYLTHIDAEVEGDTHFPDYEPDDWESV
FSEFHDADAQNSHSYSFEILERRGELGGSGGGGSGGGGSGGGGSGGGGSGGGGSGGGGS
GGGGSGGGGSGGASSSDSPRNLEVTNATPNSLTISWDNSNYASYYRITYGETGGNSPSQELT
VPGSTYNATISGLKPGQDYIITVYAVTYRDNYSYSNLISINYRSEIDKPSQGSHHHHHH

DHFR^2-Fn3 (B22) *497 amino acids; calculated MW 53.0 kDa)*

MGEQKLISEEDLGGSGGGSGGGISLIAALAVDRVIGMENAMPWNLPADLAWFKRNTLNKPVIM
GRHTWESIGRPLPGRKNIILSSQPGTDDRVTWVKSVDEAIAAAGDVPEIMVIGGGRVYEQFLPK
AQKLYLTHIDAEVEGDTHFPDYEPDDWESVFSEFHDADAQNSHSYSFEILERRGGISLIAALAV
DRVIGMENAMPWNLPADLAWFKRNTLNKPVIMGRHTWESIGRPLPGRKNIILSSQPGTDDRVT
WVKSVDEAIAAAGDVPEIMVIGGGRVYEQFLPKAQKLYLTHIDAEVEGDTHFPDYEPDDWESV
FSEFHDADAQNSHSYSFEILERRGELGGSGGGGSGGGGSGGGGSGGGGSGGGGSGGGGS
GGGGSGGGGSGGASSSDSPRNLEVTNATPNSLTISWDDYTSASYYRITYGETGGNSPSQEFT
VPGNTYNATVSGLRPGQDYIITVYAVTYRDNYSYSNPISINYRTEIDKPSQGSHHHHHH

DHFR^2-Fn3 (NT) *(499 amino acids; calculated MW 52.7 kDa)*

MGEQKLISEEDLGGSGGGSGGGISLIAALAVDRVIGMENAMPWNLPADLAWFKRNTLNKPVIM
GRHTWESIGRPLPGRKNIILSSQPGTDDRVTWVKSVDEAIAAAGDVPEIMVIGGGRVYEQFLPK

AQKLYLTHIDAEVEGDTHFPDYEPDDWESVFSEFHDADAQNSHSYSFEILERRGGISLIAALAV

DRVIGMENAMPWNLPADLAWFKRNTLNKPVIMGRHTWESIGRPLPGRKNIILSSQPGTDDRVT

WVKSVDEAIAAAGDVPEIMVIGGGRVYEQFLPKAQKLYLTHIDAEVEGDTHFPDYEPDDWESV

FSEFHDADAQNSHSYSFEILERRGELGGSGGGGSGGGGSGGGGSGGGGSGGGGSGGGGS

GGGGSGGGGSGGASSSDSPRNLEVTNATPNSLTISWDAPAVTVRYYRITYGETGGNSPSQEF

TVPGSKSTATISGLKPGQDYTITVYAVTGRDGSPASSKPISINYRTEIDKPSQGSHHHHHH

REFERENCES

1. Csizmar, C. M.; Petersburg, J. R.; Hendricks, A.; Stern, L. A.; Hackel, B. J.; Wagner, C. R., Engineering Reversible Cell-Cell Interactions with Lipid Anchored Prosthetic Receptors. *Bioconjug Chem* **2018,** *29* (4), 1291-1301.
2. Petersburg, J.; Shen, J.; Csizmar, C. M.; Murphy, K. A.; Spanier, J.; Gabrielse, K.; Griffith, T. S.; Fife, B.; Wagner, C. R., Eradication of Established Tumors by Chemically Self-Assembled Nanoring (CSAN) Targeted T-cells. *ACS Nano* **2018**, *12* (7), 6563-6576.
3. Sulzer, B.; Perelson, A. S., Equilibrium binding of multivalent ligands to cells: effects of cell and receptor density. *Math Biosci* **1996,** *135* (2), 147-85.